Synaptotagmin 1 oligomers clamp and regulate different modes of neurotransmitter release

Erica Tagliatti[a], Oscar D. Bello[a,b,1], Philipe R. F. Mendonça[a,1], Dimitrios Kotzadimitriou[a], Elizabeth Nicholson[a], Jeff Coleman[b], Yulia Timofeeva[a,c,d], James E. Rothman[a,b,2], Shyam S. Krishnakumar[a,b,2], and Kirill E. Volynski[a,b,2]

[a]Department of Clinical and Experimental Epilepsy, UCL Queen Square Institute of Neurology, University College London, WC1N 3BG London, United Kingdom; [b]Department of Cell Biology, Yale University School of Medicine, New Haven, CT 06520; [c]Department of Computer Science, University of Warwick, CV4 7AL Coventry, United Kingdom; and [d]Centre for Complexity Science, University of Warwick, CV4 7AL Coventry, United Kingdom

Contributed by James E. Rothman, December 10, 2019 (sent for review November 21, 2019; reviewed by Yukiko Goda and Thomas H. Soellner)

Synaptotagmin 1 (Syt1) synchronizes neurotransmitter release to action potentials (APs) acting as the fast Ca^{2+} release sensor and as the inhibitor (clamp) of spontaneous and delayed asynchronous release. While the Syt1 Ca^{2+} activation mechanism has been well-characterized, how Syt1 clamps transmitter release remains enigmatic. Here we show that C2B domain-dependent oligomerization provides the molecular basis for the Syt1 clamping function. This follows from the investigation of a designed mutation (F349A), which selectively destabilizes Syt1 oligomerization. Using a combination of fluorescence imaging and electrophysiology in neocortical synapses, we show that $Syt1^{F349A}$ is more efficient than wild-type Syt1 ($Syt1^{WT}$) in triggering synchronous transmitter release but fails to clamp spontaneous and synaptotagmin 7 (Syt7)-mediated asynchronous release components both in rescue ($Syt1^{-/-}$ knockout background) and dominant-interference ($Syt1^{+/+}$ background) conditions. Thus, we conclude that Ca^{2+}-sensitive Syt1 oligomers, acting as an exocytosis clamp, are critical for maintaining the balance among the different modes of neurotransmitter release.

synaptic transmission | synaptotagmin | C2B domain | fusion clamp

Tightly regulated synaptic release of neurotransmitters forms the basis of neuronal communication in the brain. Synaptotagmin 1 (Syt1) plays a key role in this process, both as the major Ca^{2+} sensor for fast synchronous action potential (AP)-evoked transmitter release and as an inhibitor of spontaneous and delayed evoked asynchronous release. Syt1 is an integral membrane protein of synaptic vesicles containing a large cytosolic part composed of 2 tandemly arranged Ca^{2+}-binding C2 domains (C2A and C2B). The C2B domain also binds SNARE (soluble *N*-ethylmaleimide–sensitive factor attachment protein receptor) complexes and acidic lipids on the presynaptic membrane, and thus supports the generation and maintenance of the readily releasable pool (RRP) of vesicles docked at the synaptic active zone (1–3). Action potential-evoked depolarization triggers opening of presynaptic voltage-gated Ca^{2+} channels, resulting in a transient and spatially restricted increase of $[Ca^{2+}]$ at the vesicular release sites. Upon Ca^{2+} binding, the adjacent aliphatic loops on Syt1 C2 domains insert into the presynaptic membrane and this triggers rapid (submillisecond timescale) fusion of RRP vesicles (4, 5).

In physiological conditions, Syt1 also acts as a suppressor (or "clamp") of spontaneous transmitter release (that occurs in the absence of neuronal spiking) and of the delayed lasting increase in vesicular exocytosis that follows APs (asynchronous release). Indeed, at many synapses, genetic deletion of Syt1 not only abolishes the fast synchronous release component but also leads to a several-fold enhancement of spontaneous and asynchronous release (6–8). Similarly, deletion of the SNARE-binding presynaptic protein complexin partially abrogates the clamping phenotype, suggesting that a synergistic action of both Syt1 and complexin is required for the fusion clamp (9, 10). However, the precise molecular mechanism of the Syt1-mediated clamp remains the subject of debate (11, 12).

We have recently demonstrated that isolated cytoplasmic portions of Syt1 readily polymerize into ring-like oligomers in vitro (13, 14). Syt1 oligomerization is triggered by binding of PIP_2 (phosphatidylinositol 4,5-bisphosphate) or ATP to a conserved polybasic motif in the C2B domain, which has been implicated in vesicle docking both in vitro and in vivo (14). The Syt1 oligomers formed on membrane surfaces are sensitive to Ca^{2+} and readily dissociate as the Ca^{2+}-binding loops located at the dimer interface (Fig. 1*A*) reorient and insert into the membrane (13, 14).

To assess whether Syt1 oligomers have a physiological role, we designed a targeted mutation (F349A) that specifically destabilizes Syt1 oligomerization in vitro, without affecting other critical molecular properties, namely Ca^{2+} and SNARE binding and membrane interaction (15). Previously, we found that rescue overexpression of $Syt1^{F349A}$ in nonneuronal neuroendocrine PC12 cells increased constitutive exocytosis, effectively occluding Ca^{2+}-stimulated vesicular release (15). We also observed that the F349A mutation abrogates the ability of Syt1 to clamp Ca^{2+}-independent fusion in a reconstituted single-vesicle fusion assay (16). Together, these findings prompted the hypothesis that Syt1 oligomers acting as a fusion clamp could play a key role in Ca^{2+} regulation of vesicular fusion.

Significance

Release of neurotransmitters relies on submillisecond coupling of synaptic vesicle fusion to the triggering signal: AP-evoked presynaptic Ca^{2+} influx. The key player that controls exocytosis of the synaptic vesicle is the Ca^{2+} sensor synaptotagmin 1 (Syt1). While the Ca^{2+} activation of Syt1 has been extensively characterized, how Syt1 reversibly clamps vesicular fusion remains enigmatic. Here, using a targeted mutation combined with fluorescence imaging and electrophysiology, we show that the structural feature of Syt1 to self-oligomerize provides the molecular basis for clamping of spontaneous and asynchronous release but is not required for triggering of synchronous release. Our findings propose a mechanistic model that explains how Syt1 oligomers regulate different modes of transmitter release in neuronal synapses.

Author contributions: E.T., O.D.B., P.R.F.M., J.E.R., S.S.K., and K.E.V. designed research; E.T., O.D.B., P.R.F.M., D.K., and E.N. performed research; J.C. contributed new reagents/analytic tools; E.T., O.D.B., P.R.F.M., D.K., E.N., Y.T., J.E.R., S.S.K., and K.E.V. analyzed data; and E.T., J.E.R., S.S.K., and K.E.V. wrote the paper.

Reviewers: Y.G., RIKEN Center for Brain Science; and T.H.S., University of Heidelberg.

The authors declare no competing interest.

[1]O.D.B. and P.R.F.M. contributed equally to this work.

[2]To whom correspondence may be addressed. Email: james.rothman@yale.edu, s.krishnakumar@ucl.ac.uk, or k.volynski@ucl.ac.uk.

This article contains supporting information online at https://www.pnas.org/lookup/suppl/doi:10.1073/pnas.1920403117/-/DCSupplemental.

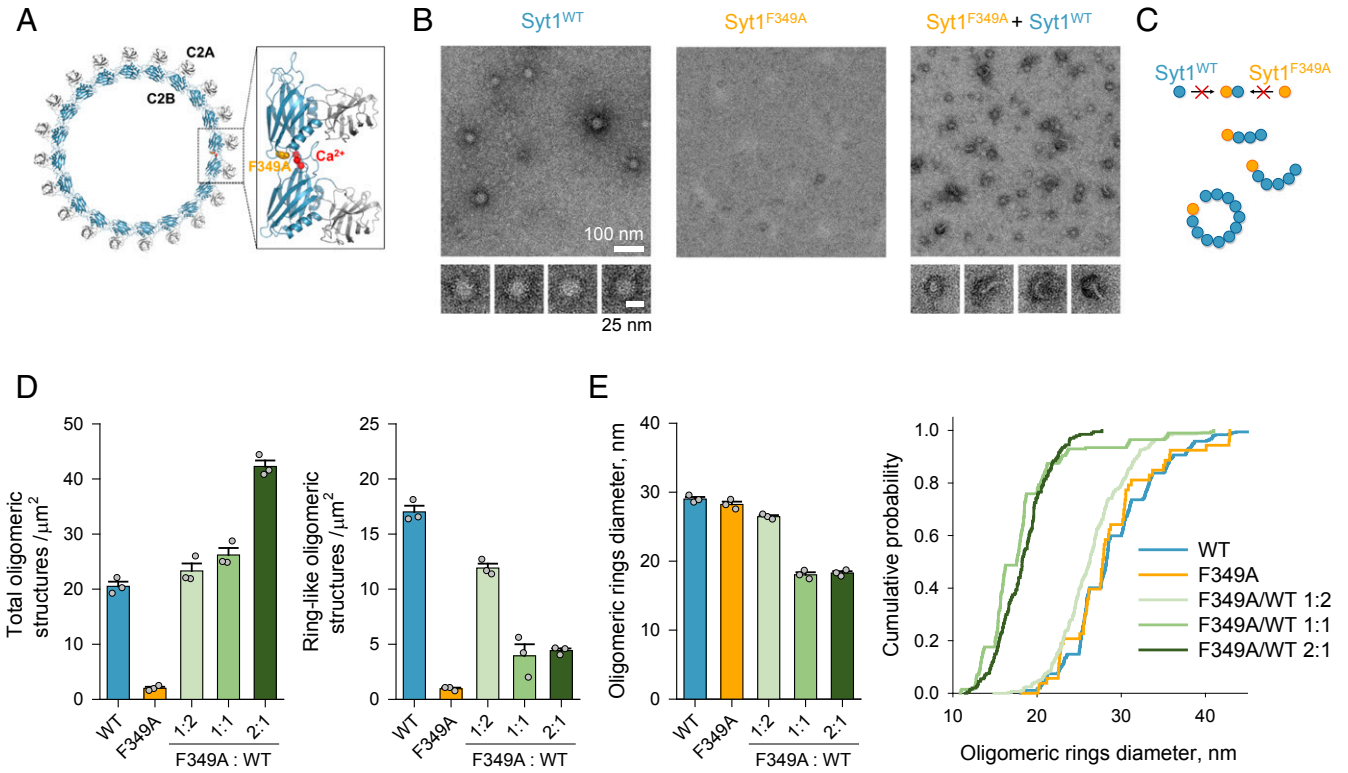

Fig. 1. Dominant effect of F349A mutation on Syt1 oligomerization. (*A*) Reconstruction of the Syt1 ring-like oligomers shows that the interaction of the C2B domains (blue) drives the oligomerization, with the Ca^{2+}-binding loops (red) locating to the dimer interface. The F349A mutation designed to disrupt oligomerization (15) is shown in orange. (*B* and *C*) Negative-stain EM analysis shows that $Syt1^{F349A}$ by itself does not form oligomeric structures, and when mixed with $Syt1^{WT}$ (1:1 molar ratio) dominantly interferes with the formation of Syt1 oligomeric rings (*B*), likely by acting as a chain terminator of the polymerization reaction (*C*). (*D*) $Syt1^{F349A}$, when mixed with $Syt1^{WT}$, increases the total number of oligomeric structures (*Left*) but critically lowers the number of ring-like oligomeric structures (*Right*) in a dose-dependent manner. (*E*) The resultant oligomeric ring-like structures (in 1:1 and 2:1 $Syt1^{F349A}/Syt1^{WT}$ mixtures) were smaller in size (average outer diameter ~20 nm) as compared with ring-like oligomers observed with $Syt1^{WT}$ or $Syt1^{F349A}$ alone (~30-nm outer diameter). Bar graphs in *D* and *E* represent mean ± SEM. The cumulative plot in *E* contains data on the size of ring-like particles pooled from all experiments. Detailed statistical analysis including the number of independent experiments is shown in *SI Appendix*, Table S1.

Here we systematically investigated the role of Syt1 oligomerization in regulating different modes of neurotransmitter release in neuronal synapses in culture using the oligomer-destabilizing F349A mutant. We found that $Syt1^{F349A}$ is more efficient than wild-type Syt1 ($Syt1^{WT}$) in rescuing synchronous transmitter release from knockout ($Syt1^{-/-}$) neurons but fails to restore the clamp on asynchronous and spontaneous release. Furthermore, consistent with its dominant-interfering phenotype in vitro, overexpression of $Syt1^{F349A}$ in $Syt1^{+/+}$ neurons potentiates Syt1-mediated synchronous, Syt7-mediated asynchronous, and AP-independent spontaneous release components. Our data argue that Ca^{2+}-sensitive Syt1 oligomers act as an exocytosis clamp and thus play the major role in coordinating different modes of transmitter release in central synapses.

Results

Dominant Effect of F349A Mutation on Syt1 Oligomerization. Based on the reconstruction of the Syt1 ring-like oligomer from the electron microscopy (EM) density map, we previously designed the F349A mutation that selectively disrupts Syt1's ability to form oligomeric structures (15). Prior to testing the effect of this mutation on neurotransmitter release, we further characterized the structural properties of $Syt1^{F349A}$ protein. Negative-stain EM analysis confirmed that the $Syt1^{F349A}$ protein lacks the inherent ability to oligomerize and further revealed that it dominantly interferes with oligomerization of $Syt1^{WT}$ molecules (Fig. 1*B*). This is consistent with the model that $Syt1^{F349A}$ acts as a chain terminator of the polymerization reaction (Fig. 1*C*). With $Syt1^{WT}$ alone, we predominantly observed stable ~30-nm-diameter size ring-like oligomers. In contrast, in $Syt1^{WT}/Syt1^{F349A}$ mixtures, we found that an increasing amount of $Syt1^{F349A}$ leads to formation of fewer and smaller (~20-nm-diameter) ring-like oligomers, with a concomitant increase in short, linear, or curved polymers (Fig. 1 *D* and *E*). This effect was fully actualized starting with a 1:1 $Syt1^{WT}/Syt1^{F349A}$ mixture.

Disruption of Syt1 Oligomerization Increases Release in Response to Single Action Potentials. To assess the impact of interfering with Syt1 oligomerization on vesicle exocytosis, we compared the functional effects of $Syt1^{F349A}$ and $Syt1^{WT}$ expression in either Syt1-deficient ($Syt1^{-/-}$) or $Syt1^{+/+}$ neurons (rescue and dominant-interference experiments, respectively) (Fig. 2 and *SI Appendix*, Figs. S1 and S2). We monitored exocytosis by imaging the pH-sensitive fluorescent vesicular recycling probe synaptophysin-pHluorin (sypHy) (17) (Fig. 2). We first recorded the increase in sypHy fluorescence in response to a 100-Hz burst of 20 APs (ΔF_{20AP}), which identified active synaptic boutons and gave an estimate of the relative size of the RRP at different synapses (18). We also monitored the increase of sypHy fluorescence after cessation of the stimulation and used this as a measure of the delayed asynchronous release component (ΔF_{asynch}). Finally, we measured the presynaptic sypHy response (averaged over 10 trials) to single AP stimulation (ΔF_{1AP}), and estimated the average release probability of individual RRP vesicles as $p_v = \Delta F_{1AP}/\Delta F_{20AP}$ (Fig. 2*A*) (18). We verified (using the v-ATPase inhibitor bafilomycin) that our estimates of the relative RRP size and of the asynchronous

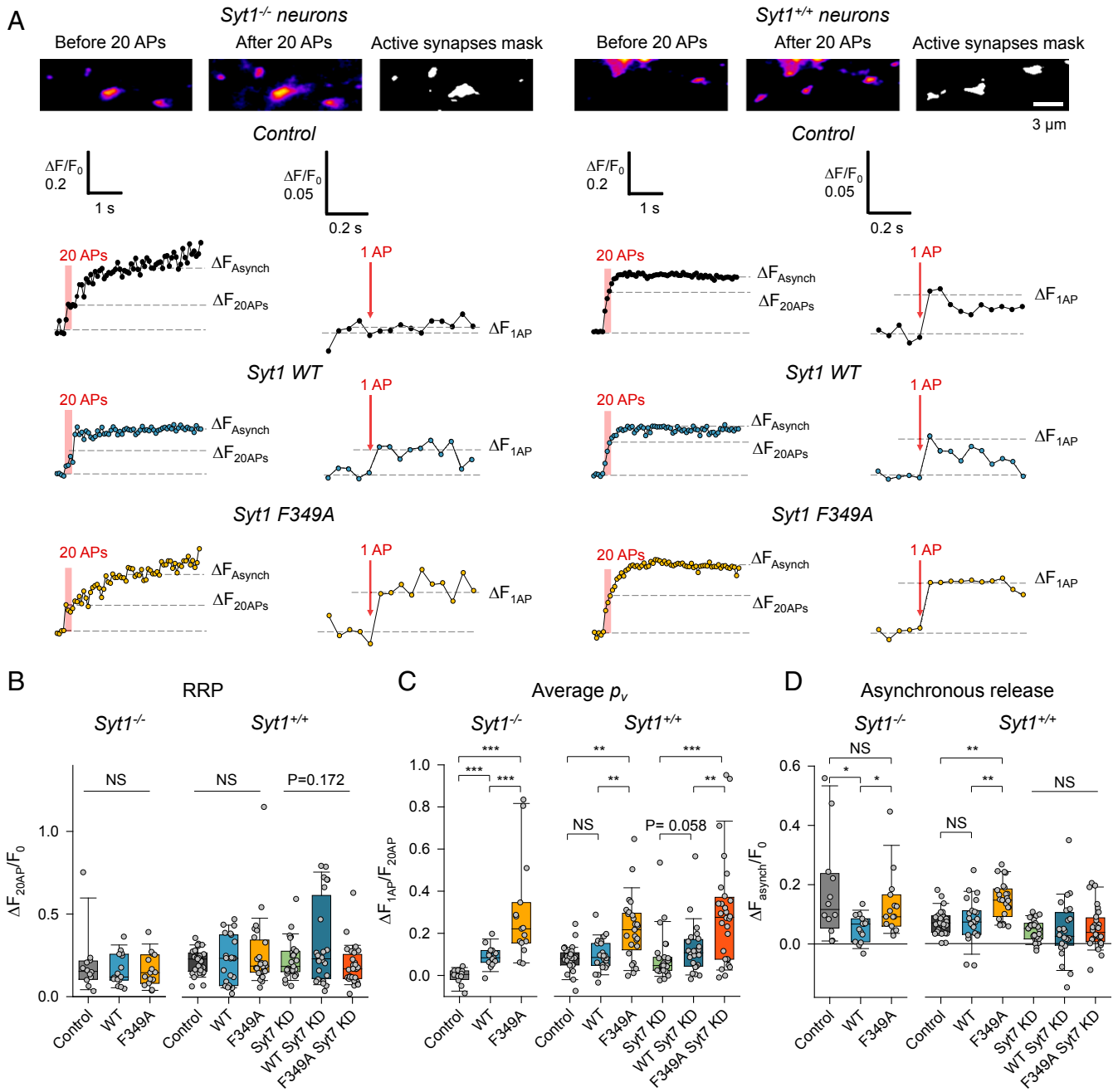

Fig. 2. Disruption of Syt1 oligomerization increases release in response to single APs and abolishes clamping of Syt7-mediated asynchronous release. (*A*, *Top*) Representative sypHy fluorescence images in untransduced Syt1$^{-/-}$ and Syt1$^{+/+}$ neurons illustrating identification of active synaptic boutons using 100-Hz stimulation of 20 APs. (*A*, *Bottom*) Representative sypHy fluorescence traces from experiments in Syt1$^{-/-}$ and Syt1$^{+/+}$ neurons designed to determine the effect of F349A mutation on the relative RRP size (ΔF_{20AP}), average release probability of RRP vesicles in response to a single AP ($p_v = \Delta F_{1AP}/\Delta F_{20AP}$) (18), and the asynchronous release component (ΔF_{asynch}) (see *Methods* for details). (*B–D*) Summary box-and-dot plots showing that overexpression of Syt1^{F349A} does not change the RRP size (*B*) but increases p_v (*C*) and the Syt7-mediated asynchronous release component (*D*) in both rescue (Syt1$^{-/-}$) and dominant-interference (Syt1$^{+/+}$) experiments. $^*P < 0.05$, $^{**}P < 0.01$, $^{***}P < 0.001$; NS, $P > 0.2$; ANOVA on ranks (*B* and *D*) and Mann–Whitney *U* test (*C* and *D*). Detailed statistical analysis including the number of independent experiments is reported in *SI Appendix*, Table S1.

release after the burst (deduced from ΔF_{20AP} and ΔF_{asynch}, respectively) were not affected by synaptic vesicle endocytosis in both Syt1$^{-/-}$ and Syt1$^{+/+}$ neurons (*SI Appendix*, *Discussion* and Figs. S3 and S4).

ΔF_{20AP} responses were similar in Syt1^{WT}- and Syt1^{F349A}-expressing synapses on both Syt1$^{-/-}$ and Syt1$^{+/+}$ backgrounds, suggesting that oligomerization of Syt1 does not have a direct effect on the RRP size (Fig. 2*B*). In line with the previously reported inhibition of synchronous transmitter release triggered by single spikes in Syt1-deficient synapses (19, 20), we could not detect a sypHy fluorescence increase in response to single AP stimulation in Syt1$^{-/-}$ neurons (Fig. 2 *A* and *C*). However, Syt1^{WT} fully rescued the release triggered by single spikes to the same level as in wild-type Syt1$^{+/+}$ neurons (Fig. 2*C*). Syt1^{F349A} was approximately twofold more efficient in rescuing release than the WT construct. Similarly, expression of Syt1^{F349A} in Syt1$^{+/+}$ neurons resulted in

a comparable increase of p_v (Fig. 2*C*). The observed gain-of-function phenotype of Syt1^{F349A} suggests that Syt1 oligomerization negatively regulates vesicular release triggered by single spikes.

Disruption of Syt1 Oligomerization Abolishes Clamping of Syt7-Mediated Delayed Asynchronous Release after the Action Potential Burst. ΔF_{asynch} was approximately twofold higher in Syt1$^{-/-}$ than in Syt1$^{+/+}$ synapses (Fig. 2*D*), in line with the reported potentiation of asynchronous transmitter release in Syt1$^{-/-}$ neurons (6). Expression of Syt1^{WT} on a Syt1$^{-/-}$ background restored the clamping of the asynchronous release component, but Syt1^{F349A} failed to do so. Correspondingly, overexpression of Syt1^{F349A} on a Syt1$^{+/+}$ background resulted in approximately twofold potentiation of ΔF_{asynch} in comparison with the untransduced control and Syt1^{WT} overexpression (Fig. 2*D*). Considering that asynchronous release in central synapses is largely mediated by the high-affinity Ca^{2+} sensor Syt7 (6, 21), we tested the effect of F349A mutation in Syt7 knockdown (KD) neurons. The increase of ΔF_{asynch} induced by the F349A mutation was occluded by siRNA-induced KD of Syt7 (Fig. 2*D* and *SI Appendix*, Fig. S5). This result indicates that Syt1 oligomers clamp the Syt7-mediated asynchronous release component.

Differential Effects of Syt1^{F349A} on Synchronous and Asynchronous Release Components during Repetitive Stimulation. The majority of the release triggered by single spikes in glutamatergic neocortical synapses is tightly synchronized to APs (22). However, due to the limited temporal resolution of sypHy imaging experiments (~50 to 100 ms), it was initially unclear to what extent the increase in p_v observed in Syt1^{F349A}-expressing neurons (Fig. 2*C*) was due to an increase of synchronous or asynchronous release components.

To address this question, we used the recently generated fluorescence glutamate sensor SF-iGluSnFR.A184V (iGluSnFR) optimized for fast optical imaging of vesicular exocytosis (23). We first established a whole-cell current-clamp recording in an iGluSnFR-expressing neuron and then imaged AP-evoked release (triggered by somatic current injections) in tens of individual boutons supplied by its axon at a rate of ~6 ms per frame (Fig. 3*A* and Movie S1). We used 51 × 5-Hz stimulation to identify all boutons (including those with low release probability) and to measure the changes in synchronous and asynchronous release during repetitive spiking. To determine the precise timing of release events, we applied a deconvolution procedure that took into account the temporal profile of uniquantal release events (*Methods*). The responses at each release site that occurred within 3 frames (~18 ms) after a given spike were classified as synchronous events and the rest as asynchronous events (red arrows, Fig. 3*A*). The amplitude of the signals after deconvolution also allowed us to determine the quantal content of each release event.

With the first AP of the burst, the synchronous component accounted for over 95% of all release in both Syt1^{WT}- and Syt1^{F349A}-overexpressing Syt1$^{+/+}$ neurons. In line with the sypHy experiments, the F349A mutation caused an ~1.35-fold increase in the average number of quanta released with the first spike (Fig. 3*B*; using the bouton as a unit of replication), albeit somewhat smaller than the increase in p_v (~2-fold) estimated using sypHy imaging (Fig. 2*C*). We observed a similar trend using the recorded neuron as the unit of replication (Fig. 3*C*; albeit falling short of significance, $P = 0.12$). It should be noted that the difference in the magnitude of the effect of the F349A mutation in sypHy and iGluSnFR imaging experiments is likely due to the differences in the types of boutons sampled. While both high and low release probability boutons are sampled in the sypHy experiment (identified with a high-frequency burst of APs), the low release probability boutons may be missed in the iGluSnFR experiment. During repetitive stimulation the synchronous release showed prominent short-term depression [characteristic of neocortical glutamatergic synapses in culture (22)], effectively occluding the difference between Syt1^{WT}- and Syt1^{F349A}-expressing synapses.

In contrast, the asynchronous release component progressively increased during the stimulation, with ~1.6-fold stronger potentiation in Syt1^{F349A}- than in Syt1^{WT}-expressing neurons (Fig. 3 *B* and *C*). Taken together, the sypHy and iGluSnFR experiments show that destabilization of Syt1 oligomers by the F349A mutation potentiates both Syt1-mediated synchronous and Syt7-mediated asynchronous release. Thus, we conclude that Syt1 oligomers act as negative regulators of both components of AP-evoked release.

Syt1 Oligomerization Is Required for Clamping Spontaneous Release. Lastly, we determined the effect of the F349A mutation on spontaneous release in the absence of APs. We recorded miniature excitatory postsynaptic currents (mEPSCs) in the whole-cell voltage-clamp configuration in the presence of the Na^+ channel blocker tetrodotoxin (Fig. 4). The mEPSC frequency in Syt1$^{-/-}$ neurons was several-fold higher than that in Syt1$^{+/+}$ neurons, consistent with the proposed role of Syt1 in clamping spontaneous release (7, 8). The clamp on spontaneous release was rescued in Syt1$^{-/-}$ neurons by expression of Syt1^{WT} but not Syt1^{F349A}. Correspondingly, overexpression of Syt1^{F349A} on a Syt1$^{+/+}$ background resulted in approximately twofold potentiation of spontaneous release (Fig. 4*B*). These results argue for the critical role of Syt1 oligomerization in clamping spontaneous neurotransmitter release. The average amplitudes of mEPSCs were similar across all of the conditions tested (Fig. 4*C*), ruling out any possible contribution of event misdetection to the observed differences in mEPSC frequencies.

Discussion

In this report, we applied the direct classical approach based on testing the effects of a targeted mutation that specifically disrupts a given molecular property—Syt1 oligomerization—to establish its physiological role in regulation of synaptic neurotransmitter release.

We report that Syt1 oligomerization provides the molecular basis for clamping of spontaneous and asynchronous release but is not required for triggering of synchronous release. This argues that clamping and activation functions of Syt1 can be separated. In fact, we find that destabilization of Syt1 oligomers with the Syt1^{F349A} mutant potentiates synchronous release triggered by single APs with no detectable changes in the RRP size. This suggests that Syt1 oligomerization is part of the fusion clamp but is not the only mechanism at work. Indeed, Syt1 monomers, as well as complexin and Syt7, have been shown to contribute to synaptic vesicle fusion clamping and to the maintenance of the RRP (9, 10, 24, 25).

How do Syt1 oligomers contribute to clamping of different modes of transmitter release? A recent X-ray structure of the Syt1–complexin–SNARE complex has provided an insight into the architecture of the prefusion state of these proteins (26). It reveals 2 Syt1 binding sites on each primed SNARE complex—a "primary" site, only found in Syt1, Syt2, and Syt9 isoforms that mediate fast synchronous release, and a complexin-dependent "tripartite" site, which is conserved across all synaptotagmin isoforms (*SI Appendix*, Fig. S6*A*). Syt1 mutations that disrupt either the primary or the tripartite site interaction motifs fail to rescue synchronous transmitter release and to maintain the RRP in neurons lacking endogenous Syt1 and Syt7 (26). This argues for the importance of both primary and tripartite sites for Syt1 function.

The Syt1–complexin–SNARE crystal structure can be combined with the molecular architecture of Syt1 ring-like oligomers into a

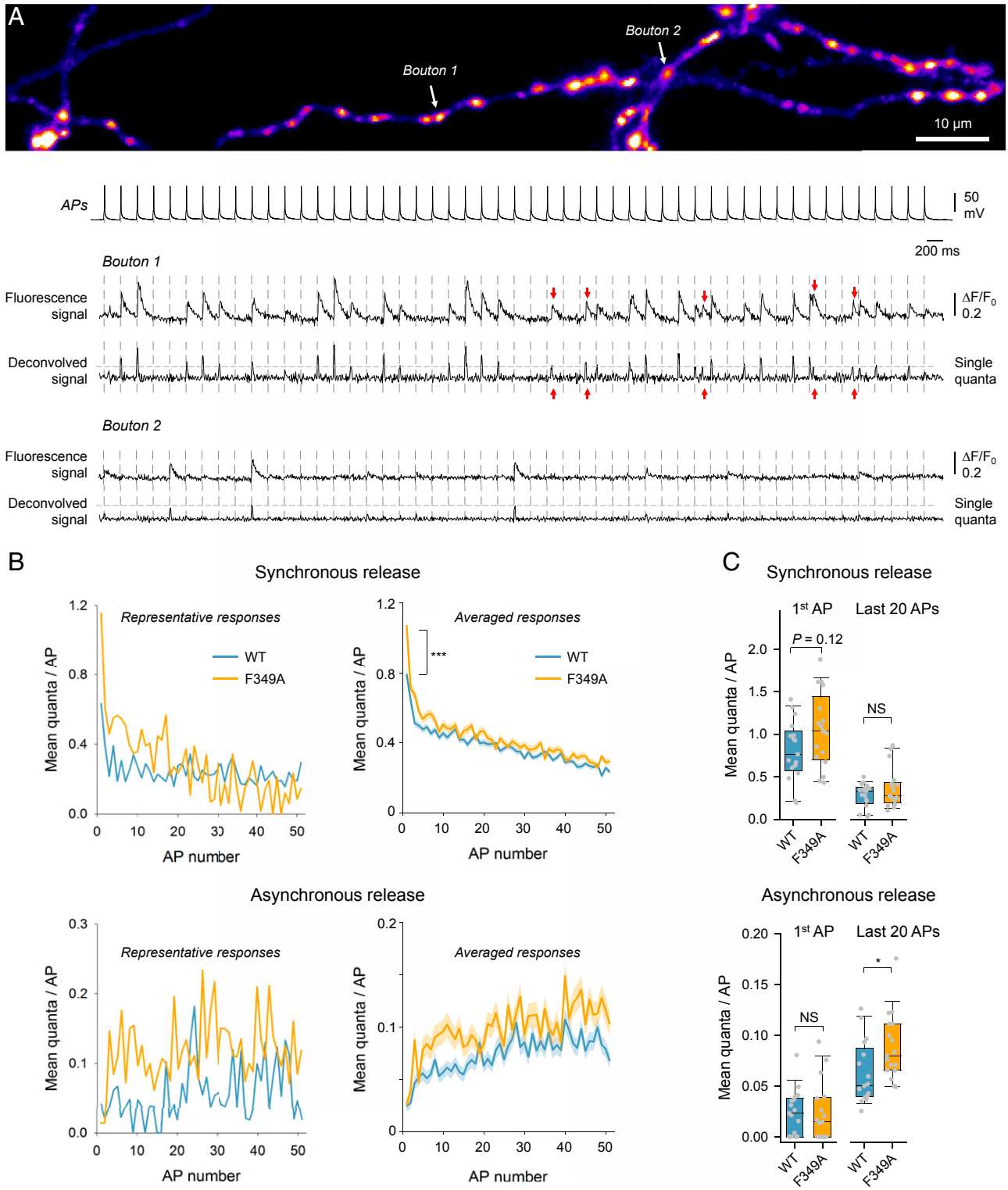

Fig. 3. Differential effects of Syt1^{F349A} on synchronous and asynchronous release components during repetitive stimulation. (*A*) Representative iGluSnFR imaging experiment in control Syt1$^{+/+}$ neurons, designed to detect quantal synchronous and asynchronous glutamate release events in individual synaptic boutons. (*A*, *Top*) Heatmap image revealing locations of glutamate release sites across the axonal arbor of a pyramidal neuron determined with 51 × 5-Hz stimulation (Movie S1). (*A*, *Bottom*) Traces, somatic APs, and iGluSnFR fluorescence responses from 2 representative boutons with high and low release probabilities. Corresponding deconvolved signals were used to estimate the quantal size (horizontal gray lines) and timing of release events (red arrows indicate asynchronous events). (*B*, *Left*) Mean quantal responses for synchronous (*Top*) and asynchronous (*Bottom*) release at each spike in 2 representative experiments recorded in Syt1$^{+/+}$ neurons overexpressing either Syt1^{WT} ($n = 56$ boutons) or Syt1^{F349A} ($n = 62$ boutons). (*B*, *Right*) Responses averaged across all boutons in all recorded cells (Syt1^{WT}, $n = 1,367$ boutons from 17 cells; Syt1^{F349A}, $n = 935$ boutons from 17 cells; shaded areas indicate SEM; ***$P < 0.001$; Mann–Whitney *U* test). (*C*) Summary plots showing the gain-of-function phenotype of the F349A mutation on synchronous release at the first spike and on asynchronous release triggered by the repetitive stimulation. Data points are mean values across all boutons (~30 to 100 range) in each recorded cell. *$P < 0.05$; NS, $P > 0.7$; Mann–Whitney *U* test. Detailed statistical analysis including the number of independent experiments is shown in *SI Appendix*, Table S1.

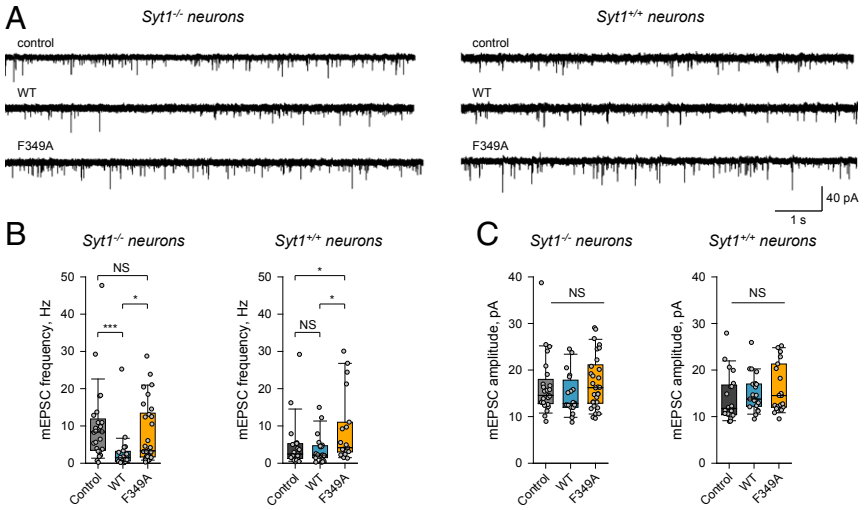

Fig. 4. Syt1 oligomerization is required for clamping spontaneous release. (*A*) Representative mEPSC traces recorded in untransduced Syt1$^{-/-}$ or Syt1$^{+/+}$ neurons (control) and in Syt1$^{-/-}$ or Syt1$^{+/+}$ neurons overexpressing either Syt1^{WT} or Syt1^{F349A}. (*B* and *C*) Quantification of the effects of Syt1^{WT} or Syt1^{F349A} overexpression on mEPSC frequency (*B*) and amplitude (*C*). Syt1^{F349A} fails to rescue the Syt1-mediated clamp of spontaneous release in Syt1$^{-/-}$ neurons and potentiates spontaneous release in Syt1$^{+/+}$ neurons, without affecting mEPSC amplitudes in all conditions. *P < 0.05, ***P < 0.001; NS, P > 0.17; Mann–Whitney U test (*B*) and ANOVA on ranks (*C*). Detailed statistical analysis including the number of independent experiments is shown in *SI Appendix*, Table S1.

working model which could explain the Syt1 clamping function in molecular terms (12). This model posits that Syt1 oligomers are formed at the interface between RRP vesicles and the presynaptic membrane, and interact with the SNAREpins as visualized in the crystal structure (*SI Appendix*, Fig. S6*B*). The SNAREpins are retained on the Syt1 C2B domain ring oligomer formed on the plasma membrane via the primary interaction site. In addition, a second independent C2B domain locates above the SNAREpin bound via the tripartite site in conjunction with complexin. As a result, the assembling SNAREpins are firmly held between 2 C2B domains and are "clamped" in position. The reversal of this dual-fusion clamp—that is, activation of release—would require complete or partial disassembly of Syt1 oligomers and the removal of the clamp at the tripartite site, which are both triggered by Ca^{2+} binding to C2 domains. It is worth noting that complexin, besides contributing toward the establishment of the tripartite clamp, might also independently block the complete assembly of the SNAREpins via its accessory helix (27). However, the precise molecular organization and the underlying mechanism are still under debate.

It is easy to imagine that Syt1 oligomers would bind SNAREs at the primary site while Syt7, Doc2B (or other Ca^{2+} sensors) could occupy the tripartite site. Thus, the dual-clamp model additionally provides a plausible explanation for how Ca^{2+}-sensitive Syt1 oligomers could dynamically regulate different modes of transmitter release triggered not only by Syt1 but also by the other Ca^{2+} release sensors (1–3, 6, 28). It is worth noting that a proportion of spontaneous release is mediated by synaptic vesicles that are molecularly distinct from those that mediate the evoked release (29). It remains to be determined whether Syt1 contributes to the release of this vesicular pool. Apart from the steric occlusion model, Syt1 oligomers are also expected to negatively regulate C2B domain membrane loop insertion and activation of the associated SNAREpins by stabilizing the Ca^{2+}-binding aliphatic loops at the dimer interface (Fig. 1*A*). This is also likely to contribute to the gating of different modes of vesicular release.

When the Syt1 oligomers are destabilized (either dynamically or constitutively with the F349A mutation), the dissociated Syt1 monomers are still expected to maintain SNAREs in the half-zippered state. A recent cryo-EM structure shows that Syt1 monomers bound to SNAREs via the primary site can still create a steric block hindering the full assembly of the associated SNAREpin, and this can be further augmented by the dual-clamp arrangement at the tripartite site (25). Nonetheless, this is expected to be a weakened clamp state, which is in line with our finding that constitutive destabilization of Syt1 oligomerization by the F349A mutation potentiates all modes of evoked, and spontaneous, release.

The local concentration of Syt1 on a docked synaptic vesicle is expected to be in the millimolar range (considering 15 to 20 copies of Syt1 localized within 5 nm of the synaptic vesicle membrane). The K_d for Syt1 oligomerization is ~10 μM (30), so it is reasonable to expect that higher-order Syt1 oligomers will form under these conditions. Furthermore, given the exceedingly high local concentration, it is possible that Syt1^{F349A} oligomers may still assemble under synaptic vesicles, though they are expected to have higher dissociation rates and thus be destabilized compared with Syt1^{WT}. In fact, Syt1^{F349A} does not completely abolish oligomerization of Syt1^{WT} when mixed together in vitro (Fig. 1*B*). On the other hand, we observe a similar loss-of-clamp phenotype in both rescue and dominant-interference experiments in neurons. This argues that formation of oligomers above a certain critical size is likely required for the Syt1-mediated clamping function.

While the precise spatial organization of Syt1 oligomers in vivo remains unclear, recent cryoelectron tomography experiments in PC12 cells suggest that fully assembled Syt1 ring-like oligomers may indeed exist on RRP vesicles (31). These experiments revealed a circular arrangement of 6 modules of the release machinery under docked synaptic-like vesicles, which is disrupted by overexpression of Syt1^{F349A}. This suggests that in addition to the key role for Syt1 oligomers in clamping of different modes of transmitter release (described in the present study), Syt1 oligomerization could also provide a framework to template and connect multiple SNAREpins to allow their cooperative function.

Methods

Lipid Monolayer Assay. Lipid monolayers were set up as described previously (13–15). Briefly, degassed ultrapure filtered water was injected through a side port to fill up 4-mm-diameter and 5-mm-depth wells in a Teflon block. The flat-water surface was coated with 0.6 μL phospholipid mixture 1-palmitoyl-2-oleoyl-*sn*-glycero-3-phosphocholine/1,2-dioleoyl-*sn*-glycero-3-phospho-L-serine

(Avanti Polar Lipids) with a molar ratio of 60:40, 0.5 mM in chloroform. The Teflon block was then stored in a sealed humidity chamber for 1 h at room temperature to allow the chloroform to evaporate. Lipid monolayers formed at the air–water interface were then recovered by placing the carbon-coated EM grids (400 mesh; Ted Pella) on top of each water droplet for 1 min. Grids were raised above the surface of the Teflon block by injecting ultrapure H_2O into the side port and then immediately lifted off the droplet. Protein mixes were diluted to 5 μM in 20 mM 3-(*N*-morpholino)propanesulfonic acid (pH 7.5), 15 mM KCl, 1 mM EDTA, 2 mM $MgAc_2$, 1 mM DTT, and 4% (wt/vol) trehalose buffer, added to the lipid monolayer on the grid, and then incubated in a 37 °C humidity chamber for 1 min. The final KCl concentration in the buffer was adjusted to 10 mM. Finally, the dried grids were negatively stained with uranyl acetate solution (1% wt/vol) and examined on an FEI Tecnai T12 microscope operated at 120 kV. The defocus range used for our data was 0.6 to 2.0 μm. Images were recorded under low-dose conditions (~20 $e^-/Å^2$) on a 4K × 4K charge-coupled device (CCD) camera (UltraScan 4000; Gatan) at a nominal magnification of 42,000×. Micrographs were binned by a factor of 2 at a final sampling of 5.6 Å per pixel on the object scale. The image analysis, including size distribution measurements, was carried out using ImageJ software (NIH). The following DNA constructs, which have been previously validated in ref. 15, were used: pCDFDuet-GST-PreScission-Syt1-C2AB-WT and Syt1-C2AB-F349A.

Neuronal Cultures. Experiments conformed to the Animals (Scientific Procedures) Act 1986, and were approved by the ethics committee of the UCL Queen Square Institute of Neurology. Primary cortical neurons were produced from either $Syt1^{+/+}$ or $Syt1^{-/-}$ mice (B6; 129S-Syt1tm1Sud/J; Jackson Laboratory) and cultured in Neurobasal A/B27-based medium (Thermo Fisher Scientific). Briefly, cortices were dissected from postnatal day 0 pups and dissociated by enzymatic digestion in 0.25% trypsin for 10 min at 37 °C and then triturated using a standard p1000 micropipette. Neurons were plated on poly-L-lysine (1 mg/mL; Sigma-Aldrich)–treated 19-mm glass coverslips at a density of 100,000 to 120,000 cells per coverslip (for imaging and electrophysiological experiments) or on poly-L-lysine (0.1 mg/mL)–treated 35-mm plastic dishes at a density of 500,000 cells per dish for Western blot analysis.

Construction of Plasmids. Syt1-Myc–tagged lentiviral constructs were generated using the pCMV-Myc-N vector (Clontech) containing full-length rat Syt1 and a preprotachykinin signal sequence cloned upstream of the Myc tag as described in ref. 15. The F349A mutation was introduced using site-directed mutagenesis (QuikChange; Agilent Technologies). Myc-tagged $Syt1^{WT}$ and $Syt1^{F349}$ sequences were then subcloned into the lentiviral vector L309, a gift from T. Südhof, Stanford University, Stanford, CA (32), under the ubiquitin promoter using BamHI and BsrGI restriction sites, thereby removing the IRES-EGFP region. For Syt7 KD experiments, the previously validated oligonucleotide sequence KD606 (5′-AAAGACAAGCGGGTAGAGAAA-3′) (24) was cloned under the U6 promoter present in L309-Myc-Syt1 constructs using AscI and PacI restriction sites. The control Syt7 KD lentiviral construct was generated by replacing Myc-tagged $Syt1^{WT}$ with the mCherry sequence under the ubiquitin promoter using BamHI and BsrGI restriction sites. To generate the mCherry-tagged Syt1 constructs, the pcDNA3 pHluorin rat Syt1 plasmid, a gift from V. Haucke, Leibniz-Forschungsinstitut für Molekulare Pharmakologie, Berlin, Germany (33), was modified by exchanging the pHluorin and mCherry sequences using HindIII and AgeI restriction sites. mCherry-tagged Syt1 WT and F349A sequences were then moved into the pCCL lentiviral backbone, a gift from S. Schorge, University College London, under the human Synapsin promoter using BamHI and SalI restriction sites. The pFU_SypHy plasmid was kindly provided by A. Maximov, The Scripps Research Institute, La Jolla, CA. The pAAV.hSynap.SF-iGluSnFR.A184V plasmid (23) was kindly provided by J. Marvin and L. Looger, Janelia Research Campus, Ashburn, VA.

Lentiviral Production and Transduction of Primary Cortical Cultures. The production of vesicular stomatitis virus-pseudotyped second- and third-generation lentiviruses was performed by cotransfection of the pFUGW/L309/PCCL-based expression vectors and 2 (pCMVdelta and pCMV-VSV-G) or 3 helper plasmids (pCMV-VSV-G, pMDLg/pRRE, pRSV-Rev) in human embryonic kidney 293T cells using Lipofectamine 2000 (Thermo Fisher Scientific) following the instructions of the manufacturer. Primary neurons were transduced at 7 d in vitro (DIV) using 10 multiplicity of infection either with viruses expressing the Myc-tagged $Syt1^{WT}$ and $Syt1^{F349A}$ (Figs. 1 and 3) or the mCherry-tagged $Syt1^{WT}$ and $Syt1^{F349A}$. Transduction efficiency (80 to 95% range) was verified using immunofluorescence analysis (*SI Appendix*, Figs. 2–5). For experiments in Fig. 1, neuronal cultures were also transduced with the sypHy-expressing lentivirus. For experiments in Fig. 2, cortical neurons were transfected at 5 DIV with the pAAV.hSynap.SF-iGluSnFR.A184V plasmid using Neuromag reagent (KC30800; OZ Biosciences). This allowed expression of the iGluSnFR probe only in a small (~3 to 5%) subpopulation of neurons, which was essential for imaging of vesicular release in individual synaptic boutons.

SypHy Imaging Experiments. All imaging and electrophysiological experiments were conducted in a custom-made open laminar flow field-stimulation chamber (0.35 mL) at 23 to 25 °C and 15 to 22 DIV. The extracellular buffer (EB1) contained 125 mM NaCl, 2.5 mM KCl, 2 mM $MgCl_2$, 2 mM $CaCl_2$, 30 mM glucose, and 25 mM Hepes (pH 7.4) (34, 35). To block recurrent activity, EB1 was supplemented with 2,3-dihydroxy-6-nitro-7-sulfamoyl-benzo[f] quinoxaline (NBQX) (10 μM; Ascent Scientific) and DL-AP5 (50 μM; Ascent Scientific). SypHy imaging was performed on an inverted Zeiss Axiovert 200 fluorescence microscope using a 63× (1.4 numerical aperture; N.A.) oil-immersion objective. Images (12-bit) were acquired using a Prime95B CMOS camera (Photometrics) coupled to a 488-nm excitation light-emitting diode (LED) light source and a 510 long-pass emission filter, with an exposure time of 50 ms. Evoked sypHy responses were recorded in an ~180 × 180-μm region of interest (ROI) typically containing 50 to 200 individual boutons. Images were analyzed using ImageJ (NIH) and MATLAB (MathWorks) custom-made software scripts. Synaptic boutons were identified by subtracting the resting sypHy fluorescence from the peak fluorescence after 100-Hz burst of 20 APs, which was previously shown to trigger release of the entire RRP of vesicles (18). This was followed by the generation of a binary mask that was used to measure the average fluorescence response in all identified boutons in each experiment (Fig. 1*C*). After subtracting the background, the data were normalized to the resting sypHy signal. The release probability of RRP vesicles was estimated by normalizing the average (10 sweeps) sypHy response to a single spike to the response to 100-Hz burst of 20 APs (18): $p_v = \Delta F_{1AP}/\Delta F_{20AP}$. We also used the increase of sypHy fluorescence measured 1.1 s after the AP burst as a lower estimate of the asynchronous release (ΔF_{asynch}, average of 8 frames between 0.9 and 1.25 s).

Potentially, both ΔF_{20AP} and ΔF_{asynch} could be affected by synaptic vesicle endocytosis and reacidification. To assess this, we carried out paired experiments with or without bafilomycin, a v-ATPase inhibitor that blocks reacidification of newly endocytosed vesicles. We recorded sypHy responses to 100-Hz stimulation of 20 APs for 100 s first in the absence and then in the presence of bafilomycin (1 μM final concentration, applied to the cells for 1 min before the recording). In some experiments, this was followed by recording sypHy responses to 1,200 APs 10-Hz stimulation. All sypHy imaging was performed with an acquisition rate of 20 Hz (50 ms per frame) with the exception of long-lasting bafilomycin experiments, where only the first 5 s of the acquisition was acquired at 20 Hz to estimate the RRP size, and then the rest of the acquisition was done at 2 Hz to minimize photobleaching.

iGluSnFR Imaging Experiments. iGluSnFR imaging was performed on an inverted Olympus IX71 fluorescence microscope equipped with a 60× (1.35 N.A.) oil-immersion objective and a QuantEM 512SC EM-CCD camera (Photometrics). iGluSnFR fluorescence was recorded using a 470-nm excitation LED and a 500- to 550-nm band-pass emission filter. Expression of the mCherry-tagged $Syt1^{WT}$ and $Syt1^{F349A}$ constructs was confirmed using a white LED combined with a 535- to 560-nm band-pass excitation filter and a 570-nm long-pass emission filter. The carbonated extracellular buffer (EB2) contained 125 mM NaCl, 26 mM $NaHCO_3$, 1.25 mM $NaHPO_4$, 2.5 mM KCl, 2 mM $CaCl_2$, 1.3 mM $MgCl_2$, and 12 mM glucose; NBQX (10 μM), DL-AP5 (50 μM), and picrotoxin (50 μM; Tocris Bioscience) were added to block the recurrent activity.

An isolated putative pyramidal-like neuron expressing iGluSnFR was whole-cell patch-clamped with a 5- to 7-MΩ fire-polished borosilicate glass pipette (current-clamp configuration) using the following intracellular solution: 105 mM K^+-gluconate, 30 mM KCl, 10 mM Hepes, 10 mM phosphocreatine-Na_2, 4 mM ATP-Mg, 0.3 mM GTP-NaH_2O, and 1 mM EGTA, balanced to pH 7.3 with KOH, −10-mV liquid junction potential. Neurons were stimulated using 15-ms current pulses (~300 pA), generating a total of 51 APs at 5 Hz. Action potential waveform recordings were obtained with an Axon Multiclamp 700B amplifier and CV-7 headstage (Molecular Devices). Signal was acquired at 20 kHz (4-kHz Bessel-filtering), with WinWCP software controlling a National Instrument board (NI USB-6221). Candidate presynaptic boutons were selected for imaging by tracing the axon from the patched neuron and identifying regions with stereotypical ~1- to 2-μm bulbous structures, usually within a 200-μm distance from the soma. An ROI of ~137 × 20 μm (512 × 75 pixels) was imaged with 6.05-ms temporal resolution, using 150 EM gain. Image acquisition was performed using μManager software (36). For each cell, from 1 to 5 different ROIs were recorded. Imaging and electrophysiological recordings were synchronized,

allowing us to identify the precise timing of the release event with respect to the presiding AP. The acquired image stack was first band-pass–filtered at 0.5 to 30 Hz (z axis) and then median-filtered (x and y axes, 3 × 3 pixels), revealing the location of the stereotypical iGluSnFR responses (Movie S1). Next, a maximal projection was produced from the filtered image stack, from which ROIs corresponding to putative boutons were selected using ImageJ software. This set of ROIs was used to extract iGluSnFR responses from the raw, unfiltered image.

To determine the timing and amplitudes of quantal releases in each bouton, the average unitary iGluSnFR response [defined as an instantaneous rise and an exponential decay $f_{\text{unitary}}(t) = \exp^{-t/\tau}$, where τ = 60 ms is the experimentally determined decay time constant] was deconvolved from the raw iGluSnFR response as $F^{-1}[F(f_{\text{iGluSnFR}}(t))/F(f_{\text{unitary}}(t))]$, where F is the discrete Fourier transform and F^{-1} is the inverse Fourier transform (MATLAB). Events were defined as synchronous if they occurred within 3 frames (~18 ms) of the preceding AP, and asynchronous in any other condition. Amplitude was estimated in quanta, which was calculated as 1) the average 5 smallest synchronous events for high release probability boutons, 2) the average 2 smallest synchronous events for low release probability boutons, or 3) the smallest event if no 2 synchronous releases were detected.

mEPSC Recording and Analysis. Spontaneous mEPSCs were recorded in EB1 supplemented with 1 μM tetrodotoxin (Tocris Bioscience), 100 μM picrotoxin, and 1 μM CGP55845 (Tocris Bioscience). Patch pipettes (8 to 12 MΩ) were fabricated from borosilicate glass capillaries using a micropipette puller (P-97; Sutter). The intracellular solution contained 125 mM CS-OH, 125 mM gluconic acid, 10 mM Hepes, 10 mM phosphocreatine-Na_2, 8 mM NaCl, 0.33 mM Na-GTP, 4 mM Mg-ATP, 0.2 mM EGTA, and 5 mM TEA-Cl (pH 7.33). Putative pyramidal cells were visualized using differential interference contrast and an inverted microscope (Axio Observer A1; Zeiss) equipped with a CMOS Prime95B camera. Postsynaptic mEPSCs were recorded in voltage-clamp mode at a holding potential of −65 mV using a MultiClamp 700B (Axon Instruments), filtered at 3 kHz (Bessel filter), and digitized at 10 kHz using an NI-DAQmx National Instruments interface card and WinEDR software (Strathclyde Electrophysiology). No correction was made for the junction potential between the patch pipette intracellular and extracellular solutions. Series resistance (R_s) was monitored every ~2 min with 10-mV hyperpolarizing steps and was not corrected. No compensation was made for whole-cell (C_m) and electrode capacitance (C_p). To confirm the AMPAR origin of the detected events in a subset of cells, the AMPA/kainate receptor antagonist NBQX (25 μM) was bath-applied at the end of the experiments. Individual mEPSC detection was performed in a single time window (30 to 120 s) at least 2 min after obtaining a whole-cell configuration, to allow for stable recording conditions. Recordings were band-pass–filtered between 4 Hz and 5 kHz (pClamp 10; Molecular Devices). Threshold criteria for mEPSC detection were amplitude >5 pA, duration 0.5 to 100 ms, with noise rejection 0.5 ms. Recordings were excluded if holding current exceeded −350 pA, R_s exceeded 35 MΩ, and/or R_s varied by >20% during the recording.

Sucrose-Based Measurements of RRP Size. As an alternative estimate of RRP size, we adapted a previously established protocol based on hyperosmotic treatment with sucrose solution (37, 38). Neuronal cultures were perfused with DL-AP5 (50 μM), picrotoxin (50 μM), and tetrodotoxin (1 μM). Putative pyramidal neurons were selected and postsynaptic currents were recorded in whole-cell configuration with a cesium gluconate-based intracellular solution (held at −60 mV, up to 40% series resistance correction, no LJP correction). EB2 supplemented with 0.5 M sucrose was locally delivered using a low-resistance borosilicate pipette (~3 MΩ), which was positioned on top of the recorded neuron and pressure-applied. RRP size was defined as the total area of the inward transient current below the steady-state baseline (achieved after a few seconds of sucrose perfusion).

Immunofluorescence Analysis. Neurons were fixed with 4% paraformaldehyde in phosphate-buffered saline (PBS) for 10 min and permeabilized with 0.1% Triton X-100 in PBS (Thermo Fisher Scientific) for 10 min. Nonspecific binding sites were blocked by incubation for 30 min with 3% BSA and 0.1% Triton X-100 in PBS before a 2-h incubation at room temperature with primary antibodies. Neurons were washed 3 times with PBS and incubated with secondary antibodies conjugated to Alexa Fluor (488, 555, or 568) for 45 min at room temperature. Coverslips were washed 3 times in PBS and mounted using a mounting media containing DAPI (Thermo Fisher; P36931) to visualize nuclei. For Syt7 KD experiments, cortical neurons were fixed with cold methanol for 7 min and then processed as described above without any permeabilization step. The following primary antibodies were used: anti-Syt1 (105 003; Synaptic Systems); anti-Myc (MA1-980; Thermo Fisher), anti-Map2 (AB5543; Millipore); anti-Syt7 (105 173; Synaptic Systems); and anti-VGlut1 (135-304; Synaptic Systems). Somatic and synaptic fluorescence intensity was quantified using ImageJ (NIH). Somatic fluorescence intensity was estimated by manual tracking of cell bodies while synaptic intensity was quantified by applying 2-μm-diameter circular ROIs over the identified synaptic boutons. For Syt7 KD experiments, a binary mask created from the Myc staining image (green channel) was applied to estimate the total Syt7 intensity (red channel). In Syt7 KD-only neurons, the binary mask was created from the mCherry image (red channel).

Excitatory synaptic density was estimated by manually counting Vglut1-positive boutons along Map2-positive branches using ImageJ software. Sholl analysis of iGluSnFR-transfected neurons was performed using the Sholl analysis plugin in ImageJ. Briefly, circles of increasing radius, originating from the center of the transfected cell body, were drawn, and the numbers of intersections between dendritic branches and the edges of the circles were used as an estimate of neuronal arborization.

Western Blotting. Cortical neurons at 16 DIV were harvested in RIPA lysis buffer [50 mM Tris·HCl, pH 7.5, 150 mM NaCl, 1% Nonidet P-40, 0.5% sodium deoxycholate, 0.1% sodium dodecyl sulfate (SDS), 1 mM EDTA, 1 mM EGTA] containing Halt protease inhibitor mixture (1 in 100; Thermo Fisher). After centrifugation at 16,000 × g for 15 min at 4 °C, samples were loaded onto an SDS/polyacrylamide gel, transferred to nitrocellulose membranes, and immunoblotted with primary antibodies followed by HRP-conjugated secondary antibodies. The following primary antibodies were used: anti-Syt1 (105 003; Synaptic Systems), anti-Syt7 (105 173; Synaptic Systems), and anti-GAPDH (glyceraldehyde 3-phosphate dehydrogenase; G8795; Sigma). Immunoreactive bands were visualized by enhanced chemiluminescence (ECL), captured using a Bio-Rad ChemiDoc reader, and analyzed using ImageLab software. Syt1 and Syt7 protein levels were normalized to the GAPDH loading control.

Statistical Analysis. The distribution of data in each set of experiments was first tested for normality using the Shapiro–Wilk test. The similarity of variances between each group of data was tested using the F test. Normally distributed data are presented as mean ± SEM; each plot also contains the individual data points. Student's t tests for group means or 1-way ANOVA were used as indicated. The datasets that failed the normality test are presented using box-and-whisker plots (box 25th to 75th percentiles, whiskers 10th to 90th percentiles); each plot also contains the individual data points. Here, Mann–Whitney U test and ANOVA on ranks were used as indicated. The detailed statistical analysis is presented in *SI Appendix*, Table S1. No statistical methods were used to predetermine sample sizes, but our sample sizes are similar to those reported in previous publications in the field (18, 26, 34, 39). In Fig. 1, data analysis was performed blind to the conditions. In Figs. 2 and 3, both data collection and analysis were performed blind to the conditions. All statistical tests were performed using SigmaPlot 11 (Systat Software).

Data Availability. All of the data are available upon request from the corresponding authors.

ACKNOWLEDGMENTS. We are grateful to D. M. Kullmann for reading the manuscript and providing critical feedback. The study was supported by the Wellcome Trust (K.E.V. and J.E.R.) and Medical Research Council (K.E.V. and Y.T.).

1. P. S. Kaeser, W. G. Regehr, Molecular mechanisms for synchronous, asynchronous, and spontaneous neurotransmitter release. *Annu. Rev. Physiol.* **76**, 333–363 (2014).
2. R. Schneggenburger, C. Rosenmund, Molecular mechanisms governing Ca(2+) regulation of evoked and spontaneous release. *Nat. Neurosci.* **18**, 935–941 (2015).
3. T. C. Südhof, Neurotransmitter release: The last millisecond in the life of a synaptic vesicle. *Neuron* **80**, 675–690 (2013).
4. B. E. Paddock *et al.*, Membrane penetration by synaptotagmin is required for coupling calcium binding to vesicle fusion in vivo. *J. Neurosci.* **31**, 2248–2257 (2011).
5. J. S. Rhee *et al.*, Augmenting neurotransmitter release by enhancing the apparent Ca^{2+} affinity of synaptotagmin 1. *Proc. Natl. Acad. Sci. U.S.A.* **102**, 18664–18669 (2005).
6. T. Bacaj *et al.*, Synaptotagmin-1 and synaptotagmin-7 trigger synchronous and asynchronous phases of neurotransmitter release. *Neuron* **80**, 947–959 (2013).
7. J. T. Littleton, M. Stern, K. Schulze, M. Perin, H. J. Bellen, Mutational analysis of *Drosophila* synaptotagmin demonstrates its essential role in Ca(2+)-activated neurotransmitter release. *Cell* **74**, 1125–1134 (1993).

8. J. Xu, Z. P. Pang, O. H. Shin, T. C. Südhof, Synaptotagmin-1 functions as a Ca^{2+} sensor for spontaneous release. *Nat. Neurosci.* **12**, 759–766 (2009).
9. S. Huntwork, J. T. Littleton, A complexin fusion clamp regulates spontaneous neurotransmitter release and synaptic growth. *Nat. Neurosci.* **10**, 1235–1237 (2007).
10. X. Yang, P. Cao, T. C. Südhof, Deconstructing complexin function in activating and clamping Ca^{2+}-triggered exocytosis by comparing knockout and knockdown phenotypes. *Proc. Natl. Acad. Sci. U.S.A.* **110**, 20777–20782 (2013).
11. A. T. Brunger, U. B. Choi, Y. Lai, J. Leitz, Q. Zhou, Molecular mechanisms of fast neurotransmitter release. *Annu. Rev. Biophys.* **47**, 469–497 (2018).
12. J. E. Rothman, S. S. Krishnakumar, K. Grushin, F. Pincet, Hypothesis—Buttressed rings assemble, clamp, and release SNAREpins for synaptic transmission. *FEBS Lett.* **591**, 3459–3480 (2017).
13. J. Wang *et al*., Calcium sensitive ring-like oligomers formed by synaptotagmin. *Proc. Natl. Acad. Sci. U.S.A.* **111**, 13966–13971 (2014).
14. M. N. Zanetti *et al*., Ring-like oligomers of synaptotagmins and related C2 domain proteins. *eLife* **5**, e17262 (2016).
15. O. D. Bello *et al*., Synaptotagmin oligomerization is essential for calcium control of regulated exocytosis. *Proc. Natl. Acad. Sci. U.S.A.* **115**, E7624–E7631 (2018).
16. S. Ramakrishnan *et al*., Synaptotagmin oligomers are necessary and can be sufficient to form a Ca^{2+}-sensitive fusion clamp. *FEBS Lett.* **593**, 154–162 (2019).
17. B. Granseth, B. Odermatt, S. J. Royle, L. Lagnado, Clathrin-mediated endocytosis is the dominant mechanism of vesicle retrieval at hippocampal synapses. *Neuron* **51**, 773–786 (2006).
18. P. Ariel, T. A. Ryan, Optical mapping of release properties in synapses. *Front. Neural Circuits* **4**, 18 (2010).
19. M. Geppert *et al*., Synaptotagmin I: A major Ca^{2+} sensor for transmitter release at a central synapse. *Cell* **79**, 717–727 (1994).
20. O. H. Shin, J. Xu, J. Rizo, T. C. Südhof, Differential but convergent functions of Ca^{2+} binding to synaptotagmin-1 C2 domains mediate neurotransmitter release. *Proc. Natl. Acad. Sci. U.S.A.* **106**, 16469–16474 (2009).
21. C. Chen, R. Satterfield, S. M. Young, , Jr, P. Jonas, Triple function of synaptotagmin 7 ensures efficiency of high-frequency transmission at central GABAergic synapses. *Cell Rep.* **21**, 2082–2089 (2017).
22. A. Maximov, Z. P. Pang, D. G. Tervo, T. C. Südhof, Monitoring synaptic transmission in primary neuronal cultures using local extracellular stimulation. *J. Neurosci. Methods* **161**, 75–87 (2007).
23. J. S. Marvin *et al*., Stability, affinity, and chromatic variants of the glutamate sensor iGluSnFR. *Nat. Methods* **15**, 936–939 (2018).
24. T. Bacaj *et al*., Synaptotagmin-1 and -7 are redundantly essential for maintaining the capacity of the readily-releasable pool of synaptic vesicles. *PLoS Biol.* **13**, e1002267 (2015).
25. K. Grushin *et al*., Structural basis for the clamping and Ca^{2+} activation of SNARE-mediated fusion by synaptotagmin. *Nat. Commun.* **10**, 2413 (2019).
26. Q. Zhou *et al*., The primed SNARE-complexin-synaptotagmin complex for neuronal exocytosis. *Nature* **548**, 420–425 (2017).
27. C. G. Giraudo, W. S. Eng, T. J. Melia, J. E. Rothman, A clamping mechanism involved in SNARE-dependent exocytosis. *Science* **313**, 676–680 (2006).
28. K. E. Volynski, S. S. Krishnakumar, Synergistic control of neurotransmitter release by different members of the synaptotagmin family. *Curr. Opin. Neurobiol.* **51**, 154–162 (2018).
29. D. M. Ramirez, M. Khvotchev, B. Trauterman, E. T. Kavalali, Vti1a identifies a vesicle pool that preferentially recycles at rest and maintains spontaneous neurotransmission. *Neuron* **73**, 121–134 (2012).
30. J. Wang *et al*., Circular oligomerization is an intrinsic property of synaptotagmin. *eLife* **6**, e27441 (2017).
31. X. Li *et al*., Symmetrical organization of proteins under docked synaptic vesicles. *FEBS Lett.* **593**, 144–153 (2019).
32. Z. P. Pang, P. Cao, W. Xu, T. C. Südhof, Calmodulin controls synaptic strength via presynaptic activation of calmodulin kinase II. *J. Neurosci.* **30**, 4132–4142 (2010).
33. M. K. Diril, M. Wienisch, N. Jung, J. Klingauf, V. Haucke, Stonin 2 is an AP-2-dependent endocytic sorting adaptor for synaptotagmin internalization and recycling. *Dev. Cell* **10**, 233–244 (2006).
34. Y. S. Ermolyuk *et al*., Differential triggering of spontaneous glutamate release by P/Q-, N- and R-type Ca^{2+} channels. *Nat. Neurosci.* **16**, 1754–1763 (2013).
35. Y. S. Ermolyuk *et al*., Independent regulation of basal neurotransmitter release efficacy by variable Ca^{2+} influx and bouton size at small central synapses. *PLoS Biol.* **10**, e1001396 (2012).
36. A. D. Edelstein *et al*., Advanced methods of microscope control using μManager software. *J. Biol. Methods* **1**, 10 (2014).
37. S. Chang, T. Trimbuch, C. Rosenmund, Synaptotagmin-1 drives synchronous Ca^{2+}-triggered fusion by C_2B-domain-mediated synaptic-vesicle-membrane attachment. *Nat. Neurosci.* **21**, 33–40 (2018).
38. C. Rosenmund, C. F. Stevens, Definition of the readily releasable pool of vesicles at hippocampal synapses. *Neuron* **16**, 1197–1207 (1996).
39. Q. Zhou *et al*., Architecture of the synaptotagmin-SNARE machinery for neuronal exocytosis. *Nature* **525**, 62–67 (2015).